1

2

3

Ultraviolet light degrades the mechanical and

structural properties of human stratum corneum.

Z.W. Lipsky and G. K. German

7

8

9

10

11   **Running head:** UV degrades human stratum corneum

12   **Abbreviations:** Ultraviolet (UV), Stratum Corneum (SC), Relative Humidity (RH), Desmoglein 1 (Dsg

13   1)

14

1   **Abstract**

2   Prolonged exposure of human skin to sunlight causes photodamage, which induces the early onset of

3   wrinkles and increased tissue fragility. While solar ultraviolet (UV) light is considered to have the most

4   damaging effect, the UV range that is most harmful remains a topic of significant debate. In this study, we

5   take a first step towards elucidating biomechanical photoageing effects by quantifying how exposure to

6   different UV ranges and dosages impacts the mechanical and structural properties of human stratum

7   corneum (SC), the most superficial skin layer. Mechanical testing reveals that irradiation of isolated

8   human SC to UVA (365 nm), UVB (302 nm), or UVC (265 nm) light with dosages of up to 4000 J/cm^2

9   notably alters the elastic modulus, fracture stress, fracture strain, and work of fracture. For equivalent

10   incident dosages, UVC degrades SC the greatest. However, upon discounting reflected and transmitted

11   components of the incident light, a generalized scaling law relating the photonic energy absorbed by the

12   SC to the energy cost of tissue fracture emerges. This relationship indicates that no one UV range is more

13   damaging than another. Rather, the magnitude of absorbed UV energy governs the degradation of tissue

14   mechanical integrity. Subsequent structural studies are performed to elucidate the cause of this

15   mechanical degradation. UV absorption scales with the spatial dispersion of desmoglein 1 (Dsg 1), a

16   component of corneocyte cell-cell junctions, away from intercellular sites. Combining both scaling laws,

17   we establish a mechanical-structural model capable of predicting UV induced tissue mechanical integrity

18   from Dsg 1 dispersion.

1   **Statement of Significance**

2   Photoageing from the sun can produce early onset of skin wrinkles and an increase in tissue fragility that

3   heightens the risk of rupture. While solar ultraviolet (UV) light is considered to have the most damaging

4   effect, the UV range that is most harmful remains a topic of significant debate. In this study, we elucidate

5   photoageing effects by quantifying how exposure to different UV ranges and dosages impacts the

6   mechanical and structural properties of human stratum corneum (SC), the most superficial skin layer.

7   Results establish a mechanical-structural model that relates the amount of UV energy absorbed by the

8   tissue, irrespective of UV range, to the energy cost of tissue fracture and spatial dispersion of desmoglein

9   1.

1   ## 1. INTRODUCTION

2   Solar radiation is comprised of wavelengths ranging between 220 (ultraviolet (UV)) and 3200 nm

3   (infrared)(1). Due to its greater photon energy, the impact of UV radiation on skin is the most commonly

4   examined, however studies have explored the effects of both visible and infrared radiation(2–4). UV light

5   exposure has been linked with numerous health benefits such as increased vitamin D production and

6   phototherapy of skin conditions such as eczema(5, 6). However, the health risks of UV overexposure are

7   far more pervasive. UV exposure is associated with accelerated skin ageing(7), sunburn(8), and the

8   promotion of skin cancers such as basel cell carcinomas, squamous cell carcinomas, and malignant

9   melanomas(9). UV induced skin damage can be directly caused by DNA absorption of UV light, resulting

10   in the formation of photolesions such as cyclobutane pyrimidine dimers or (6,4) photoproducts(8, 10–13),

11   or indirectly through the generation of reactive oxygen species, which create oxidative stresses that

12   damage DNA, proteins, and lipids(8, 14, 15). The range of UV light exposure can also influence the

13   method and level of skin damage(11).

14   UV light is broken up into four distinct ranges: UVA (315-400 nm), UVB (280-315 nm), UVC(200-280

15   nm) and vacuum-UV (100-200 nm). Sunlight is comprised only of UVA and UVB light; UVC and

16   vacuum-UV are fully attenuated by the atmosphere(16). However, exposure of skin to UVC light can

17   occur when using welding equipment, sunbeds, or working within biosafety cabinets(17–19). In terms of

18   overall damaging effects on full thickness skin, the World Health Organization defines UVC as the most

19   damaging(20). However, different UV ranges do not impact skin tissue equally; UV light has wavelength-

20   dependent penetration depths. While longer wavelength UVA can reach deep into the dermis, UVB and

21   UVC light are primarily absorbed by the epidermis(21). As such, consideration for which tissue layer is

22   affected needs to be accounted for. Moreover, reports of skin damage from different UV light ranges is

23   evaluated primarily from a biological standpoint. Here damage is characterized by its impact on cellular

24   DNA(13, 15, 22–24) and carcinogensis(25–28), rather than the potential for UV light to physically

25   degrade skin integrity. While studies have explored UV light induced changes in skin elasticity(29, 30),

1   and UVB's effect on the mechanical properties of the most superficial skin layer, the stratum corneum

2   (SC)(31), the relative impact of the different UV ranges on the structural and mechanical integrity of

3   human skin remains unclear, as does the mechanism of degredation. In this study, we provide initial

4   insight into the comparative damaging effects of different UV ranges by exploring how various UVA,

5   UVB, and UVC light dosages change the mechanical and structural properties of human SC.

6   **2.   MATERIALS AND METHODS**

7   **2.1 Stratum corneum isolation.**

8   Full thickness 36 yrs. female breast skin specimens ($n = 3$) were received from Yale Pathology Tissue

9   Services (New Haven, CT) within 24 hr. of elective surgery. Breast tissue was chosen because it is

10   typically exposed only to low levels of solar UV exposure. An exempt approval (3002-13) was obtained

11   to perform research using de-identified tissue samples pursuant to the Department of Health and Human

12   Services (DHHS) regulations, 45 CFR 46.101:b:4. SC was isolated using a standard heat bath and trypsin

13   technique(32–34). Once isolated, SC sheets were placed on plastic mesh, rinsed in deionized water, and

14   dried for 48 hr. at room temperature and humidity. For uniaxial mechanical testing, SC samples were cut

15   to a uniform 7 x 20 mm size ($n = 142$ total samples used for the study). For immunostaining studies,

16   samples were cut to a uniform 3 mm diameter circle ($n = 26$ total samples used for the study). While full

17   thickness skin exhibits mechanical anisotropy (35, 36), SC tissue exhibits isotropic mechanical

18   properties(37, 38). As such, the orientation of SC samples cut from the isolated sheet are unimportant.

19   **2.2 Ultraviolet Irradiation.**

20   UV irradiation of SC samples was performed using a UV Lamp (8 Watt EL Series, Analytik Jena US

21   LLC, Upland, CA) with stand. For mechanical testing, SC samples were exposed to UVC (265 nm

22   narrowband), UVB (302 nm narrowband) or UVA (365 nm narrowband) light for periods equating to

23   incident light dosages of 10, 100, 200, 400, 800 and 4000 J/cm^2. For structural studies, SC samples were

24   exposed to UVC, UVB or UVA light for periods equating to incident light dosages of 100, 200, 400, and

25   800 J/cm^2. For samples positioned 76 mm from the light source, the average intensities of the UVA,

1   UVB, and UVC lamp bulbs are $1.5\,\text{mW/cm}^2$, $1.6\,\text{mW/cm}^2$, and $1.8\,\text{mW/cm}^2$ respectively (39). To

2   achieve equal dosages across the three UV ranges, exposure times were varied. For instance, a dosage of

3   $10\,\text{J/cm}^2$ required an exposure time of 111 min for UVA, 104 min for UVB, and 92 min for UVC. SC

4   samples exposed only to ambient UV light were used for controls.

5   **2.3 Mechanical characterization.**

6   After UV irradiation, samples were equilibrated for 24 hr. to either 25 or 100% relative humidity (RH)

7   before testing. Equilibration to low or high RH conditions were achieved by placing specimens

8   respectively in an airtight container filled with desiccant (Drierite 10-2 mesh, W.A. Hammond Drierite

9   Company, Xenia, OH) or a hydration cabinet (F42072-1000, Secador, Wayne, NJ) with a base filled with

10 deionized water. In both cases, RH conditions were monitored throughout the equilibration period using a

11 hygrometer with probe (445815, Extech Instruments, Nashua, NH)). After equilibration, the mechanical

12 properties of samples were evaluated using a uniaxial tensometer (UStretch, CellScale, Waterloo, ON,

13 Canada) equipped with a 4.4 N load cell. The ends of each SC sample were taped to prevent slippage of

14 the sample in the tensometer grips, leaving an exposed area of 7 x 10 mm. Individual SC samples were

15 mounted into opposing tensometer grips, initially separated by 10 mm. Samples were strained until

16 rupture at a constant strain rate of $0.012\ \text{s}^{-1}$; similar to rates used in previous mechanical studies of

17 skin(35). Tensile forces and grip separation were recorded at a frequency of 5 Hz. After mechanical

18 testing, the average thickness of the ruptured SC sample was quantified using optical microscopy. Optical

19 thickness measurements were taken a distance from the crack interface to prevent measuring reduced

20 thicknesses arising from plastic deformation. Combinations of sample dimensions, and recorded force-

21 displacement data were then used to derive engineering stress-strain curves, from which the average

22 elastic modulus, fracture stress, fracture strain and work of fracture were extracted ($3 \leq n \leq 9$

23 independent samples for each UV range, dosage, and humidity).

24

25

1   **2.4 Desmoglein 1 dispersion analysis**

2   Irradiated and control samples (3 mm diameter circle, $n = 2$ for each condition) were first incubated with

3   an anti-demoglein 1 (Dsg1) mouse monoclonal antibody (651110, Progen, Heidelberg, Germany) at a

4   1:500 ratio antibody to phosphate-buffered saline (PBS) at 4°C overnight (40, 41). Samples were then

5   washed three times with PBS before being incubated in a 1:200 ratio of Alexa-Fluor 488 labeled goat

6   anti-mouse IgG antibody (A-11029, Introgen, Carlsbad, CA) to PBS for 1 hr. at room temperature.

7   Samples were then rewashed in PBS three times before being placed on a glass coverslip. Images of

8   control and irradiated SC were recorded using a confocal microscope (Leica SP5, Wetzlar, Germany) and

9   63x oil objective lens, with numerical aperture of 1.4 and spatial resolution of 0.15 μm/pixel (1024 x 1024

10   pixels). A 488 nm wavelength laser was used to excite the SC samples. Fluorescent emissions were

11   recorded in the range 500 to 540 nm. Perpendicular cross sectional fluorescent intensity profiles

12   (spanning ±2.5 μm either side of the intercellular interface) across $n = 2000$ intercellular regions of

13   neighboring corneocytes ($n = 2$ samples; $n = 10$ junctions per sample; $n = 100$ cross-sections per

14   junction for each UV treatment condition) were extracted from the images. Individual profiles for each

15   UV dosage condition were normalized by peak pixel intensity, then averaged. Intercellular junctions were

16   considered to be located along the coinciding perimeters of adjacent corneocytes(42).

17   **2.5 Statistical analysis.**

18   All statistical analyses were performed using R (version 3.4.2). A 1-way ANOVA was used to test for

19   statistical significance in Figs. 1 and 2, where each UV condition (UVA, UVB, and UVC) was compared

20   to the control. Levene's and Shapiro-Wilk's tests were respectively used to determine equality of

21   variances and normality. Results in Fig. 1C (controls), Fig. 2A (UVA 10 and 200 J/cm^2), Fig. 2B (UVB

22   10 J/cm^2), Fig. 2C (UVB 800 J/cm^2, UVC 800 J/cm^2), and Fig. 2D (UVB 100 J/cm^2, UVC 800 J/cm^2)

23   were found to exhibit non-normal distributions, but equal variances. Here a Kruskal-Wallis analysis was

24   performed. Results in Fig. 1D (UVB), and Fig. 2B–D (UVB) were found to exhibit normal distributions,

25   but unequal variances. Here a 1-way ANOVA with Welch correction was performed. Post-hoc analyses

1 were performed if statistical significance levels below 5% were established. In the figures, * denotes

2 $p \leq 0.05$, ** denotes $p \leq 0.01$, and *** denotes p ≤ 0.001.

3 ### 3. RESULTS AND DISCUSSION

4 **<u>3.1 Changes in SC mechanical properties with UV irradiation.</u>**

5 Changes in the mechanical integrity of human SC with UV light range and dosage are first assessed.

6 Isolated human SC samples are irradiated with incident dosages of narrowband UVA (365 nm), UVB

7 (302 nm) or UVC (265 nm) light ranging between 0 (Control) and 4000 J/cm^2; the latter dosage being

8 equivalent to approximately 8 continual days of full-spectrum solar UVA (or 361 continual days solely at

9 365 nm) (ASTM G173-03, 2012). UV therapy treatments for various skin diseases including vitiligo,

10 pruitus, inflammatory dermatoses, and scleroderma can have cumulative dosages of up to 485 J/cm^2 for

11 narrowband UVB (311 nm)(44–46) and 2000 J/cm^2 for broadband UVA (340 to 400 nm)(47–49). Figs.

12 1A–D respectively show the average ($3 \leq n \leq 9$ samples for each UV dosage) elastic modulus, E,

13 fracture stress, σ_f, fracture strain, γ_f, and work of fracture, W_f, of irradiated samples equilibrated for 24

14 hr. to 25% relative humidity (RH) prior to mechanical testing. Fig. 1A highlights that no significant

15 change in elastic modulus occurs with either UVA or UVB irradiation, however a UVC dosage of 800

16 J/cm^2 induces a significant decrease in tissue stiffness, relative to controls. Fig. 1B shows that samples

17 undergo no significant reduction in fracture stress for UVA dosages less than 4000 J/cm^2, UVB dosages

18 less than 800 J/cm^2, and UVC dosages less than 400 J/cm^2. However, dosages at or above these levels

19 cause statistically significant decreases. Similarly, Figs. 1C and D show that significant decreases in both

20 the fracture strain and work of fracture occur with UVA dosages of 4000 J/cm^2, and both UVB and UVC
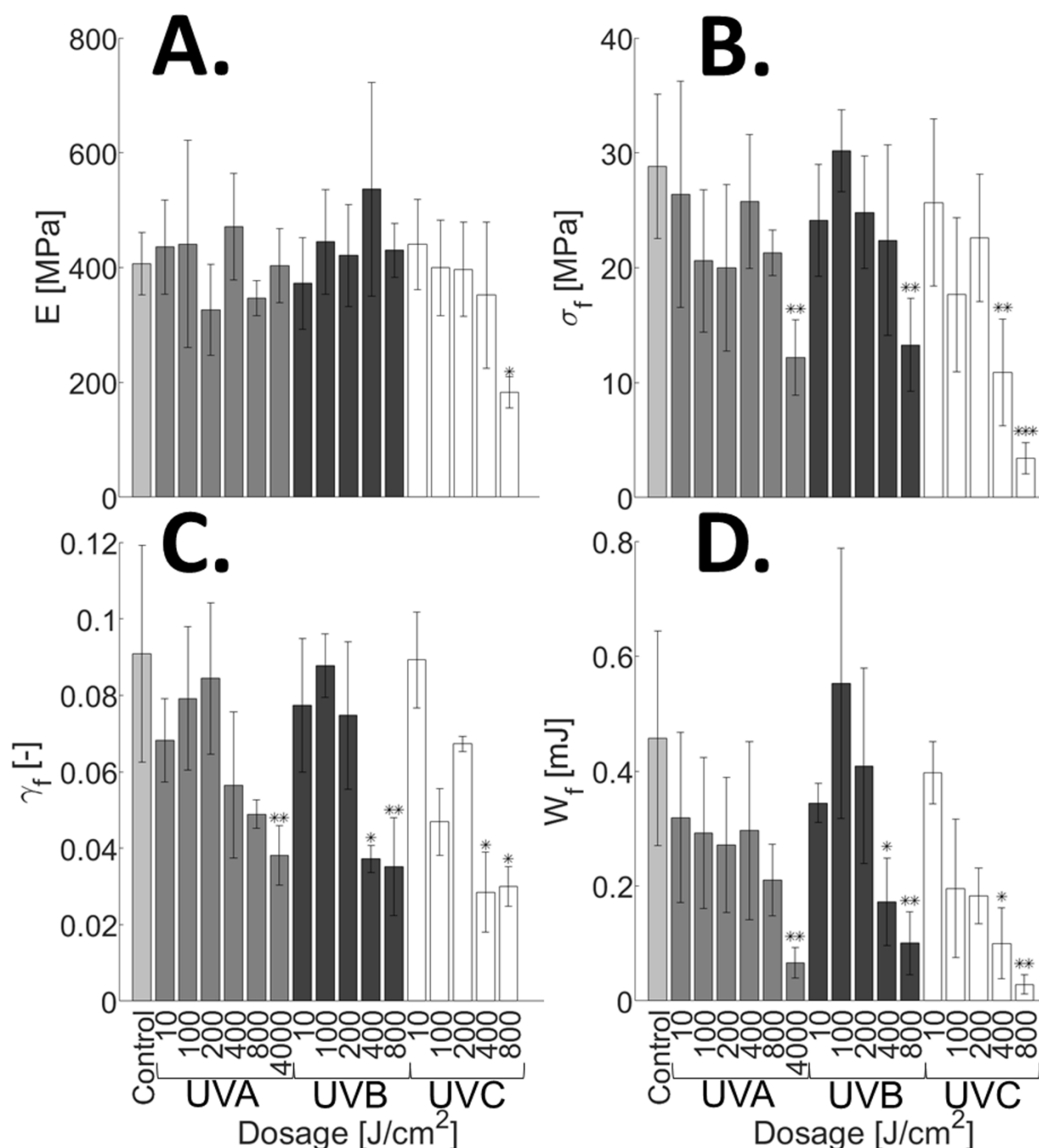
21 dosages equal to or greater than 400 J/cm^2.

Figure 1. UV induces changes in the mechanical properties of SC equilibrated to 25% RH. Average

(A) elastic modulus, E, (B) fracture stress, σ_f, (C) fracture strain, γ_f, and (D) work of fracture, W_f for

unirradiated controls (Control; light grey), UVA irradiated samples (dosage range: 10 - 4000 J/cm^2;

medium grey), UVB irradiated samples (dosage range: 10 - 800 J/cm^2; dark grey), and UVC irradiated

samples (dosage range: 10 - 800 J/cm^2; white). Bars denote average values of $3 \leq n \leq 9$ individual

1   sample measurements for each range and dosage condition. Error bars denote standard deviations. [2

2   column]

3   Figs. 2A–D show complementary mechanical results for SC samples ($3 \leq n \leq 7$ samples for each

4   dosage) equilibrated for 24 hr. to 100% RH prior to mechanical testing. In contrast to the 25% RH results

5   in Fig. 1, Figs. 2A and B highlight that no significant change in either the elastic modulus or fracture

6   stress occurs for any UV treatment. Reductions in sample fracture strain and work of fracture however

7   occur with UVA and UVB dosages of 4000 J/cm^2 and 400-800 J/cm^2 respectively, as shown in Figs. 2C

8   and D. This trend is similar to that observed for samples equilibrated to 25% RH (Fig. 1C and D),

9   however the magnitude by which these parameters decrease is notably larger for the hydrated SC.

10   Moreover, UVC dosages of 100 J/cm^2 or greater also induce statistically significant decreases. The lack

11   of statistically significant changes in elastic modulus (Fig. 1A and 2A) with UVB irradiation, along with

12   observed decreases in fracture strain with increasing UVB dosage (Fig. 1C and 2C) are consistent with
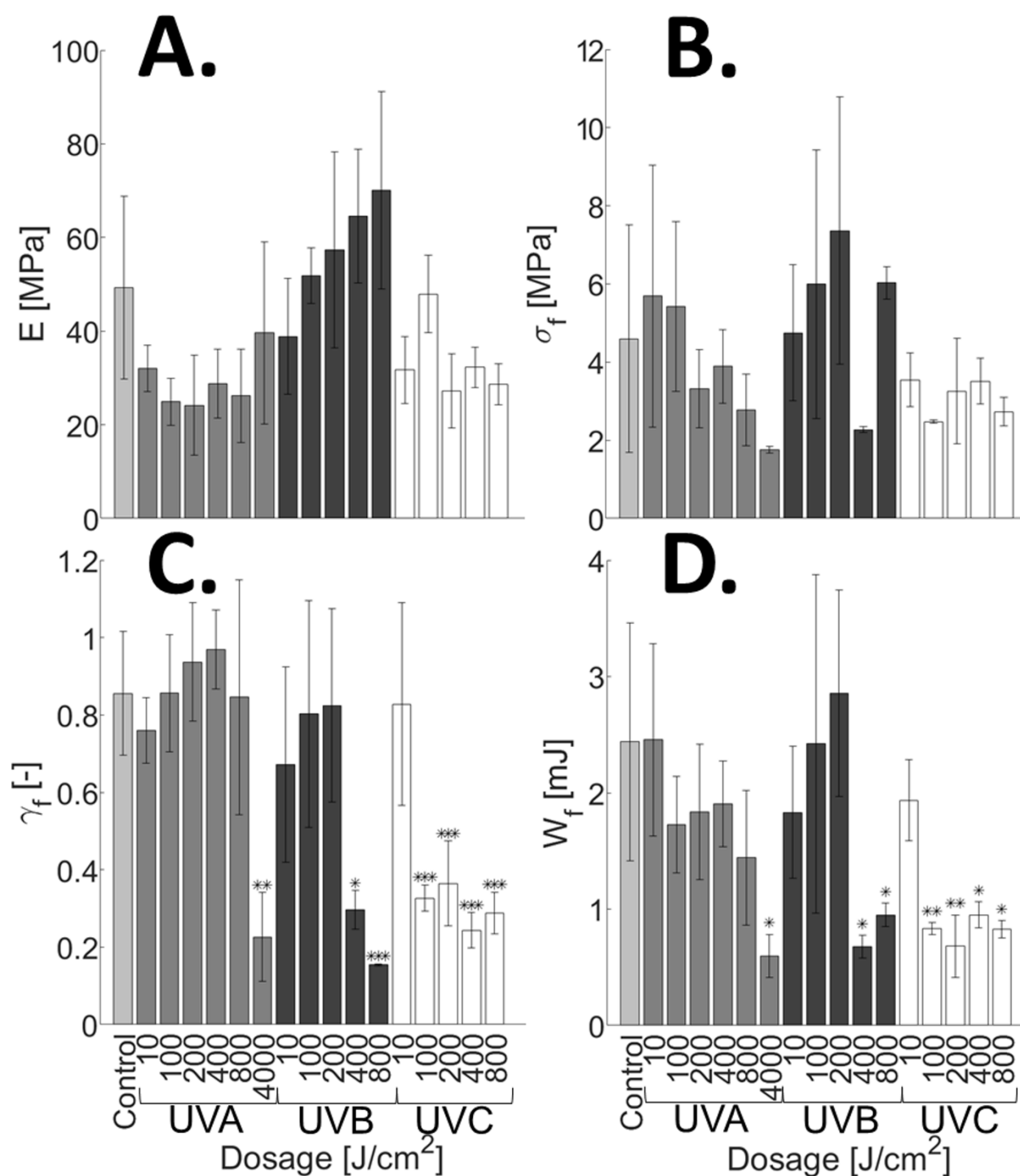
13   previous studies(31).

Figure 2. UV induces changes in the mechanical properties of SC equilibrated to 100% RH.

Average (A) elastic modulus, E, (B) fracture stress, σ_f, (C) fracture strain, γ_f, and (D) work of fracture,

W_f for unirradiated controls (Control; light grey), UVA irradiated samples (dosage range: 10 - 4000

J/cm^2; medium grey), UVB irradiated samples (dosage range: 10 - 800 J/cm^2; dark grey), and UVC

1   irradiated samples (dosage range: 10 - 800 J/cm^2; white). Bars denote average values of $3 \leq n \leq 7$

2   individual sample measurements for each range and dosage condition. Error bars denote standard

3   deviations. [2 column]

4   Results in Fig. 1 and 2 appear to highlight that for equivalent incident dosages, UVC light induces the

5   greatest loss in SC mechanical integrity, followed by UVB, then UVA. However, the incident dosage

6   does not equate with the physical energy absorbed by the SC tissue (50, 51). UV light is absorbed,

7   reflected, and transmitted through the SC; the degree with which each of these occurs is wavelength

8   dependent. Prior studies have shown that the percentage of incident UVA, UVB, and UVC light absorbed

9   by the SC is 25, 48, and 71%, respectively(50). Table S1 shows the energy physically absorbed by the SC

10   for each UV range and incident dosage. We further scrutinize our data to establish whether a relationship

11   exists between the energy absorbed by the SC, and the associated degradation in its mechanical integrity.

12   **3.2 Scaling of absorbed UV dosage with work of fracture**

13   Figs. 3 and 4 respectively show the work of fracture plotted against the physical energy absorbed by

14   individual SC samples, when equilibrated to 25 and 100% RH. Both figures reveal that irrespective of the

15   UV range used, increases in the energy absorbed by the tissue decrease the work of fracture. For each

16   figure, a relationship between the average work of fracture, W_f, and the absorbed dosage, ϕ, is

17   established by fitting the data with a nonlinear least-squares regression of the form;

$$W_f = W_0 e^{C_1 \phi}. \tag{1}$$

18

19   Best fits were made with power-law, exponential, and linear models. The exponential model in each case

20   provides the strongest correlation. The grey shaded region in each figure corresponds to the standard

21   deviation about the average work of fracture at each dosage. For tissue equilibrated to 25% RH, $W_0 =$

22   0.395 mJ and $C_1 = -3.61 \times 10^{-3}$. A p-value of $p = 5 \times 10^{-4}$ for the goodness of fit supports the notion

23   that absorbed dosage acts as a predictor of tissue mechanical integrity, with an R-squared value of 0.69.

24   Likewise, for tissue equilibrated to 100% RH, $W_0 = 2.01$ mJ and $C_1 = -1.73 \times 10^{-3}$. A p-value of

1    $p = 6 \times 10^{-3}$ is also established for the goodness of fit, with an R-squared value of 0.48. These results

2   indicate that irrespective of the UV range used, the dosage absorbed by the tissue appears to be primary

3   driving force behind the degradation of mechanical integrity.
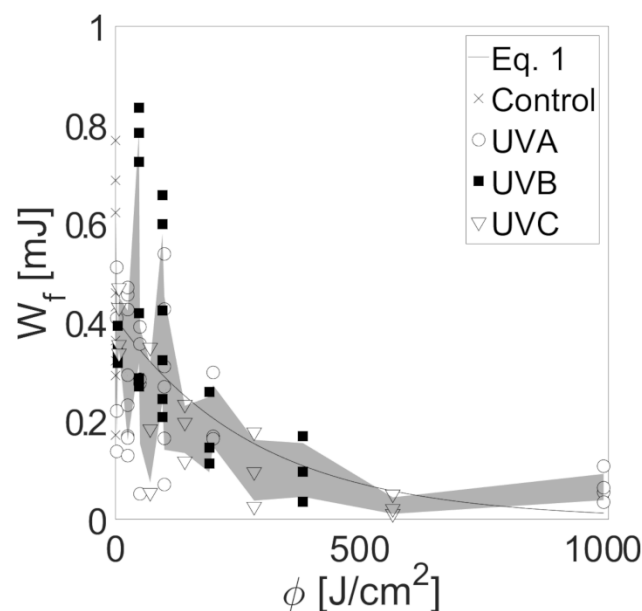
4

5   **Figure 3. Change in the work of fracture with UV energy absorbed by SC equilibrated to 25% RH.**

6   Work of fracture, W_f, of individual SC samples plotted against absorbed UV dosage, ϕ, for controls

7   (cross), and samples irradiated with UVA (open circle), UVB (filled square), and UVC (open inverted

8   triangle). An exponential least-squares best fit is represented by the solid black curve (Eq. 1, $W_0 =$

9   0.395 mJ, $C_1 = -3.61 \times 10^{-3}$). The shaded region indicates the standard deviation of the data points

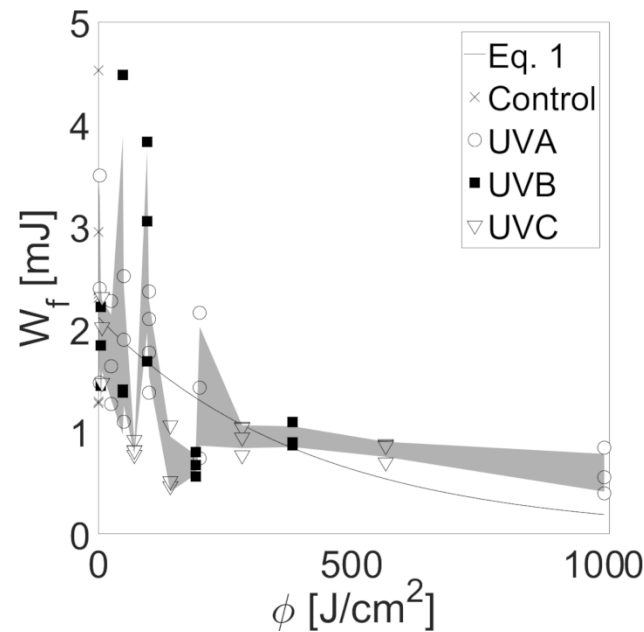10   about the mean work of fracture at each dosage. [single column]

11

1

Figure 4. Change in the work of fracture with UV energy absorbed by SC equilibrated to 100% RH. Work of fracture, W_f, of individual SC samples plotted against absorbed UV dosage, ϕ, for controls (cross), and samples irradiated with UVA (open circle), UVB (filled square), and UVC (open inverted triangle). An exponential least squares best fit is represented by the solid black curve (Eq. 1, $W_0 = 2.01$ mJ, $C_1 = -1.73 \times 10^{-3}$). The shaded region indicates the standard deviation of the data points about the mean work of fracture at each dosage. [single column]

3.3 Dispersion of intercellular desmoglein 1 with UV irradiation

While our results clearly demonstrate a loss of tissue mechanical integrity with sufficient irradiation from all UV ranges, the underlying cause of this degradation remains unclear. Previous studies have highlighted that tissue hydration is the predominant factor in altering the mechanical properties of SC(52–56). Reductions in water content are associated with increases in tissue elastic modulus(52–56), and notable decreases in the ability of SC to plastically deform prior to rupture(53, 55). While reductions in plastic deformability of SC equilibrated to 100% RH do occur with UV irradiation, as demonstrated in Fig. 5, associated increases in elastic modulus are absent (Figs. 1A and 2A). Therefore, a structural change is more likely to be the primary cause of the observed SC mechanical degradation. Alterations to

1   the corneodesmosome junctions is an attractive explanation due to its role as a major structural protein

2   that provides intercellular cohesion(57, 58). The impact of UV irradiation on changes to the presence and

3   location of desmoglein 1 (Dsg 1), a key component of corneodesmosomes, is consequently investigated

4   using immunostaining.
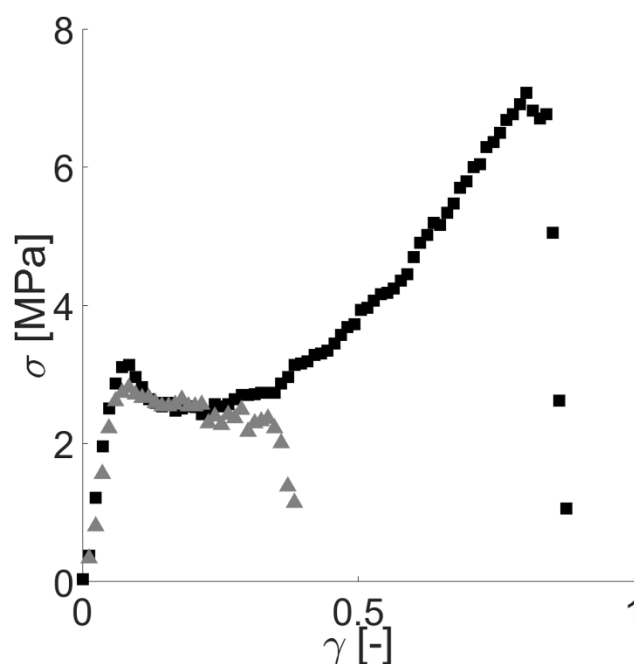
5

6   **Figure 5. Loss of SC plastic deformability with UV irradiation.** Representative stress-strain plots of an

7   unirradiated SC sample (filled squares) and a sample irradiated with 400 J/cm^2 of incident UVB light

8   (filled triangle). Both samples are equilibrated to 100% RH. [single column]

9   Fig. 6 shows the change in distribution of fluorescently tagged Dsg 1 in SC samples irradiated with

10   increasing UVB exposure. Control SC samples exposed only to ambient UV in Fig. 6A and B exhibit

11   commonly observed Dsg 1 distributions, characterized by small, distinct puncta surrounding the periphery

12   of corneocytes(40, 41, 59). Incident UVB dosages of 100 J/cm^2 (Fig. 6C and D) and 200 J/cm^2 (Fig. 6E

13   and F) display similar distributions. However Fig. 6G–J show that with incident UVB dosages of 400

14   J/cm^2 or greater, Dsg 1 lose their distinctive puncta morphology, and become more dispersed.

15   Distribution changes in Dsg 1 with UVB exposure has been cited previously with organotypic cultures,

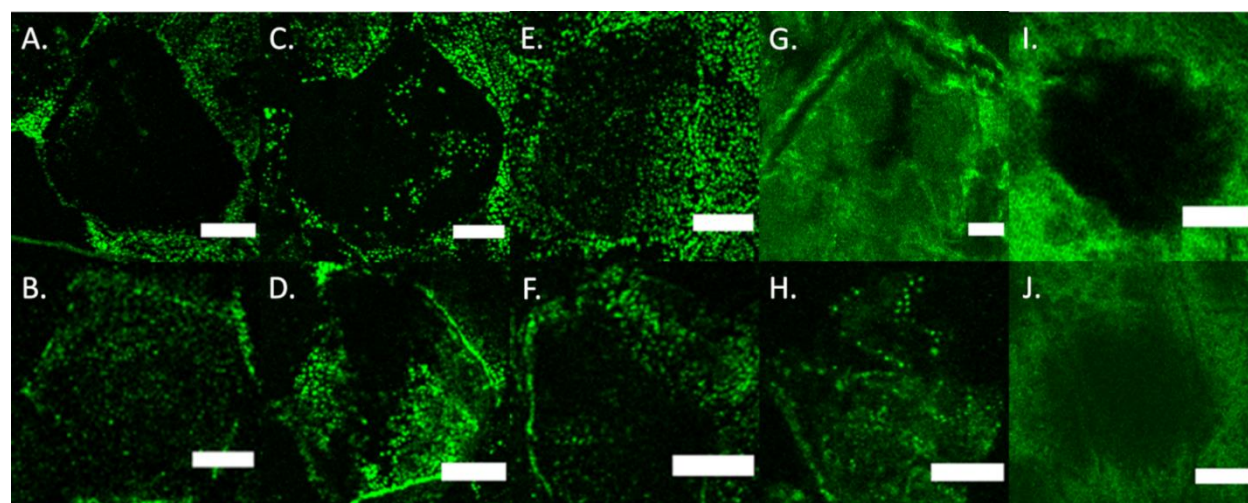16   but not to our knowledge with *ex vivo* human SC(59).

Figure 6. Confocal images showing changes in fluorescently tagged desmoglein (Dsg 1) distributions with increasing UVB dosage. Dsg 1 fluorescent images (from n=2 individual samples per condition) of control samples (A,B) and samples irradiated with an incident dosage of 100 J/cm^2 (C,D), 200 J/cm^2 (E,F), 400 J/cm^2 (G,H), and 800 J/cm^2 UVB (I,J). (*Scale bar*) 10 μm. [2 column]

The progressive dispersion of Dsg 1 is further quantified across all UV types (UVA, UVB and UVC) and dosages (0-800 J/cm^2) by characterizing the average fluorescent normalized pixel intensity (*NPI*) profiles perpendicularly across intercellular junctions. Average *NPI* profiles for each UV range and dosage are established from $n = 2000$ intercellular junction profiles (n=2 samples; n=10 junctions per sample; n=100 cross-sections per junction). Profiles from UVB irradiated samples are displayed in Fig. 7A–E. UVA and UVC irradiated profiles are provided in Fig. S1A–D and E–H respectively in the Supporting Material. All cross-sectional profiles, irrespective of UV type and dosage, exhibit peak *NPI* values at or near the center of the cross-sectional profile, coincident with the cell-cell interface. However, while intensity profiles exhibit a narrow peak at the cell-cell interface for UVB dosages of 200 J/cm^2 or less (Fig. 7A–C), consistent with dense localized puncta, greater dosages (Fig. 7D and E) exhibit notably wider peaks, indicative of dispersion. UVA and UVC irradiated samples also exhibit this trend, with profile peaks widening with UVA dosages greater than or equal to 800 J/cm^2 (Fig. S1D) and UVC dosages greater than or equal to 200 J/cm^2 (Fig. S1F–H). These results indicate that increasing dosages

1   result in increased dispersion of desmoglein for all UV ranges. To better understand this dispersion, NPI

2   profiles are fitted with a double gaussian function of the form,

3
$$NPI = \frac{1}{\sigma_1\sqrt{2\pi}}e^{-\frac{1}{2}(\frac{x}{\sigma_1})^2} + \frac{1}{\sigma_2\sqrt{2\pi}}e^{-\frac{1}{2}(\frac{x}{\sigma_2})^2},$$
(2)

4   where σ_i is the standard deviation and x denotes the lateral position across the averaged NPI profile

5   ($-2.5 \leq x \leq 2.5$ μm). The best-fit model to the control treatment profile is shown as the dotted-line in Fig.

6   7A. The inner and outer gaussian components of Eq. 2 are also plotted in Fig. 7A as dashed and solid

7   curves, respectively. We employ the standard deviation of the inner gaussian function to characterize the

8   dispersion of desmoglein, which we denote the dispersion index, DI. Fig. 7F plots DI against the

9   absorbed UV dosage, ϕ, irrespective of UV type. Similar to Fig. 3 and 4, an exponential function of the

10   form,

11
$$DI = DI_0 e^{C_2\phi}$$
(3)

12   is found to provide the best fit to the data. For the regression, $DI_0 = 0.199$ and $C_2 = 4.27 \times 10^{-3}$. A p-

13   value of $p = 7 \times 10^{-4}$ for the goodness of fit supports the absorbed dosage acting as a predictor of Dsg 1

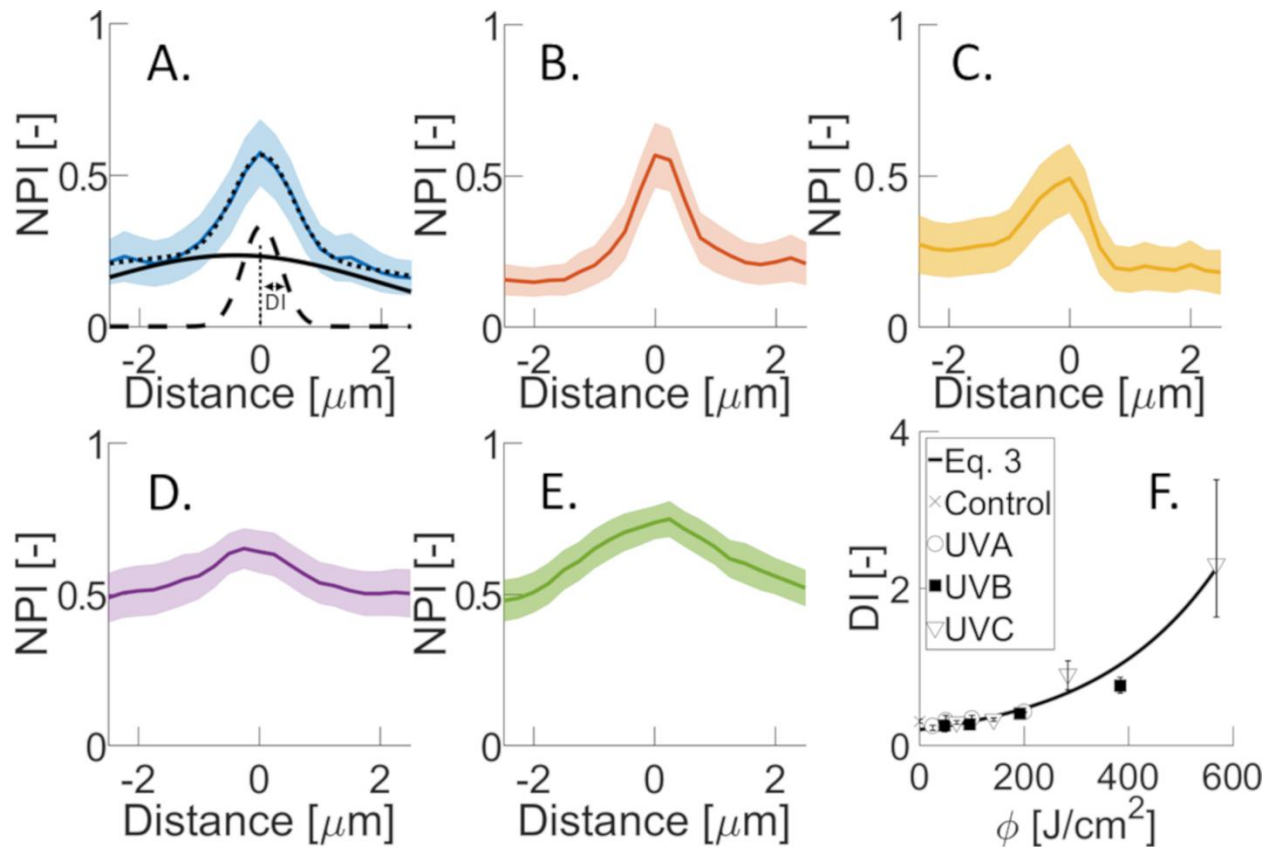14   distribution, with an R-squared value of 0.96.

15

Figure 7. **Changes in averaged normalized pixel intensity (*NPI*) profiles across intercellular corneocyte junctions with increasing UVB dosage.** (A) control samples (blue line), (B) 100 J/cm^2 incident dosage (red line), (C) 200 J/cm^2 incident dosage (yellow line), (D) 400 J/cm^2 incident dosage (purple line), and (E) 800 J/cm^2 UVB incident dosage (green line). Shaded regions correspond to the standard error about the mean curve. Eq. 2 is used to fit average *NPI* profiles. The black dotted line denotes the best fit to the average control *NPI* profile in panel A. The two individual composite gaussian distributions of Eq. 2 are also represented in this panel by black solid- and dashed-lines. The inner gaussian (black dashed-line) is used to establish the dispersion index (*DI*), equivalent to the standard deviation of the distribution. (F) Change in dispersion index, *DI*, with UVA (open circle), UVB (filled square), and UVC (open inverted triangle) energy absorbed by SC. An exponential least-squares best fit to all the data points is represented by the solid black curve. Error bars denote standard deviations. [2 column]

1   Changes in both the average work of fracture (Fig. 3 and 4), W_f, and structural dispersion index (Fig. 7F),

2   DI, with absorbed UV dosage, ϕ, exhibit exponential relationships. Combining Eq. 1 and 3, we establish

3   a power law expression relating structural and mechanical parameters of the form,

$$W_f = W_0 \left(\frac{DI}{DI_0}\right)^{\alpha}. \tag{5}$$

5   where $\alpha = C_1/C_2$. For SC samples equilibrated to 25% RH, $\alpha = -0.845$. This structure-mechanical

6   relationship highlights that the mechanical integrity of the SC tissue scales with near inverse

7   proportionality to the dispersion of intercellular junction proteins away from intercellular interfaces. We

8   restrict this model to tissue equilibrated to dry (25% RH conditions) conditions because all UV irradiation

9   protocols were performed on dry tissue samples to minimize surface, unbound, and bound water(60, 61)

10   altering the absorption, reflection, and transmission of UV(51, 62–64). Moreover, SC equilibrated to a

11   lower relative humidity is more physiologically consistent in-vivo SC tissue (20-40% RH indoors(65);

12   30-80% RH outdoors(66)).

13   **4.   Conclusion**

14   In this article, we quantify the impact of UV range and dosage on the mechanical and structural

15   degradation of isolated human stratum corneum (SC). For equivalent incident dosages, UVC light causes

16   the greatest loss in mechanical integrity of the tissue, followed by UVB and UVA. This is due to the

17   greater radiation energy UVC. However, when discounting reflected and transmitted components of the

18   incident light, a scaling law relationship between the energy absorbed and the work of SC fracture

19   emerges. This relationship highlights that no one UV range is more damaging than another. Rather, the

20   amount of energy absorbed governs the loss of tissue mechanical integrity. Further structural studies

21   reveal that desmoglein 1 (Dsg 1), a major component of corneodesmosomes, becomes dispersed with UV

22   exposure away from intercellular sites. Upon relating the mechanical and structural models, a near inverse

23   scaling law is revealed. This suggests that a simple immunostaining assay could therefore be employed to

24   quantify UV induced tissue damage.

1 We anticipate that UV light induced increases in protease activity could contribute to the observed

2 structural changes in Dsg 1 within corneodesmosomes, resulting in mechanical degradation. Stratum

3 corneum serine proteases that hydrolyze corneodesmosome components such as Dsg 1 exhibit increased

4 activity with UVB exposure in cultured epidermal keratinocytes(67). While reports have shown that the

5 enzyme activity of these proteases can be modulated *ex vivo* with factors such as hydration(68) and

6 inhibitors(69, 70), future studies should determine if similar increases in enzyme activity with UV

7 irradiation are seen in *ex vivo* SC. In addition, the scaling relationships established in this study should be

8 further tested. The validity of using absorbed energy and structural protein dispersion as a predictor of

9 biomechanical photoaging should be assessed over a wider range of the electromagnetic spectrum and in

10 deeper skin layers, perhaps through biomechanical testing and immunostaining of progressively thicker

11 skin specimens that retain epidermal, then dermal tissue.

12 **AUTHOR CONTRIBUTION**

13 G.K.G. designed the research. Z.W.L. performed the experiments and analyzed the data. Both authors
14 wrote the article.

15 **ACKNOWLEDGEMENTS**

18 **REFERENCES**

19 1.   Valley, S.L. 1965. Handbook of geophysics and space environments. Air Force Cambridge

20   research labs hanscom AFB MA.

21 2.   Kollias, N., and A. Baqer. 1984. An experimental study of the changes in pigmentation in human

22   skin in vivo with visible and near infrared light. Photochem. Photobiol. 39: 651–659.

23 3.   Lee, J.H., M.R. Roh, and K.H. Lee. 2006. Effects of infrared radiation on skin photo-aging and

24   pigmentation. Yonsei Med. J. 47: 485–490.

4. Cho, S., M.H. Shin, Y.K. Kim, J.-E. Seo, Y.M. Lee, C.-H. Park, and J.H. Chung. 2009. Effects of infrared radiation and heat on human skin aging in vivo. J. Investig. Dermatol. Symp. Proc. 14: 15–19.

5. Moan, J., A.C. Porojnicu, A. Dahlback, and R.B. Setlow. 2008. Addressing the health benefits and risks, involving vitamin D or skin cancer, of increased sun exposure. Proc. Natl. Acad. Sci. U. S. A. 105: 668–73.

6. Reynolds, N.J., V. Franklin, J.C. Gray, B.L. Diffey, and P.M. Farr. 2001. Narrow-band ultraviolet B and broad-band ultraviolet A phototherapy in adult atopic eczema: A randomised controlled trial. Lancet. 357: 2012–2016.

7. Panich, U., G. Sittithumcharee, N. Rathviboon, and S. Jirawatnotai. 2016. Ultraviolet radiation-induced skin aging: The role of DNA damage and oxidative stress in epidermal stem cell damage mediated skin aging. Stem Cells Int. 2016.

8. D'Orazio, J., S. Jarrett, A. Amaro-Ortiz, and T. Scott. 2013. UV radiation and the skin. Int. J. Mol. Sci. 14: 12222–12248.

9. Böni, R., C. Schuster, B. Nehrhoff, and G. Burg. 2002. Epidemiology of skin cancer. Neuroendocrinol. Lett. 23: 48–51.

10. Pfeifer, G.P. 1997. Formation and Processing of UV Photoproducts: Effects of DNA Sequence and Chromatin Environment. Photochem. Photobiol. .

11. Besaratinia, A., J. -i. Yoon, C. Schroeder, S.E. Bradforth, M. Cockburn, and G.P. Pfeifer. 2011. Wavelength dependence of ultraviolet radiation-induced DNA damage as determined by laser irradiation suggests that cyclobutane pyrimidine dimers are the principal DNA lesions produced by terrestrial sunlight. FASEB J. .

12. Jiang, Y., M. Rabbi, M. Kim, C. Ke, W. Lee, R.L. Clark, P.A. Mieczkowski, and P.E. Marszalek.

1   2009. UVA Generates Pyrimidine Dimers in DNA Directly. Biophysj. 96: 1151–1158.

2   13. Pfeifer, G.P., and A. Besaratinia. 2012. UV wavelength-dependent DNA damage and human non-

3   melanoma and melanoma skin cancer. Photochem. Photobiol. Sci. 11: 90–97.

4   14. Brem, R., P. Macpherson, M. Guven, and P. Karran. 2017. Oxidative stress induced by UVA

5   photoactivation of the tryptophan UVB photoproduct 6-formylindolo[3,2-b]carbazole (FICZ)

6   inhibits nucleotide excision repair in human cells. Sci. Rep. .

7   15. Schuch, A.P., N.C. Moreno, N.J. Schuch, C.F.M. Menck, and C.C.M. Garcia. 2017. Sunlight

8   damage to cellular DNA: Focus on oxidatively generated lesions. Free Radic. Biol. Med. 107:

9   110–124.

10   16. U.S. Department of Health and Human Services. 2000. Report on Carcinogens Background

11   Document for Ultraviolet (UV) Radiation. .

12   17. Dixon, A.J., and B.F. Dixon. 2004. Ultraviolet radiation from welding and possible risk of skin

13   and ocular malignancy. Med. J. Aust. 181: 155–157.

14   18. Zhang, M., A.A. Qureshi, A.C. Geller, L. Frazier, D.J. Hunter, and J. Han. 2012. Use of tanning

15   beds and incidence of skin cancer. J. Clin. Oncol. 30: 1588–1593.

16   19. Meechan, P.J., and C. Wilson. 2006. Use of Ultraviolet Lights in Biological Safety Cabinets: A

17   Contrarian View. Appl. Biosaf. 11: 222–227.

18   20. World Health Organization., and International Programme on Chemical Safety. 1994. Ultraviolet

19   radiation : an authoritative scientific review of environmental and health effects of UV, with

20   reference to global ozone layer depletion. .

21   21. Meinhardt, M., R. Krebs, A. Anders, U. Heinrich, and H. Tronnier. 2008. Wavelength-dependent

22   penetration depths of ultraviolet radiation in human skin. J. Biomed. Opt. 13: 44030.

22. Dong, K.K., N. Damaghi, S.D. Picart, N.G. Markova, K. Obayashi, Y. Okano, H. Masaki, S. Grether-Beck, J. Krutmann, K.A. Smiles, and D.B. Yarosh. 2008. UV-induced DNA damage initiates release of MMP-1 in human skin. Exp. Dermatol. 17: 1037–1044.

23. Kvam, E., and R.M. Tyrrell. 1997. Induction of oxidative DNA base damage in human skin cells by UV and near visible radiation. Carcinogenesis. 18: 2379–2384.

24. Tadokoro, T., N. Kobayashi, B.Z. Zmudzka, S. Ito, K. Wakamatsu, Y. Yamaguchi, K.S. Korossy, S.A. Miller, J.Z. Beer, and V.J. Hearing. 2003. UV-induced DNA damage and melanin content in human skin differing in racial/ethnic origin. FASEB J. 17: 1177–1179.

25. Ziegler, A., A.S. Jonason, D.J. Leffellt, J.A. Simon, H.W. Sharma, J. Kimmelman, L. Remington, T. Jacks, and D.E. Brash. 1994. Sunburn and p53 in the onset of skin cancer. Nature. 372: 773–776.

26. Chen, A.C., G.M. Halliday, and D.L. Damian. 2013. Non-melanoma skin cancer: Carcinogenesis and chemoprevention. Pathology. 45: 331–341.

27. Buckman, S. 1998. COX-2 expression is induced by UVB exposure in human skin: implications for the development of skin cancer. Carcinogenesis. 19: 723–729.

28. de Gruijl, F.R., H.J. Van Kranen, and L.H.F. Mullenders. 2001. UV-induced DNA damage, repair, mutations and oncogenic pathways in skin cancer. J. Photochem. Photobiol. B Biol. 63: 19–27.

29. Oba, A., and C. Edwards. 2006. Relationships between changes in mechanical properties of the skin, wrinkling, and destruction of dermal collagen fiber bundles caused by photoaging. Ski. Res. Technol. 12: 283–288.

30. Nishimori, Y., C. Edwards, A. Pearse, K. Matsumoto, M. Kawai, and R. Marks. 2001. Degenerative alterations of dermal collagen fiber bundles in photodamaged human skin and UV-irradiated hairless mouse skin: Possible effect on decreasing skin mechanical properties and

1   appearance of wrinkles. J. Invest. Dermatol. 117: 1458–1463.

31. Biniek, K., K. Levi, and R.H. Dauskardt. 2012. Solar UV radiation reduces the barrier function of human skin. Proc. Natl. Acad. Sci. 109: 17111–17116.

32. Kligman, A.M., and E. Christophers. 1963. Preparation of isolated sheets of human stratum corneum. Arch. Dermatol. 88: 702–705.

33. Liu, X., and G.K. German. 2015. The effects of barrier disruption and moisturization on the dynamic drying mechanics of human stratum corneum. J. Mech. Behav. Biomed. Mater. 49: 80–9.

34. German, G.K., E. Pashkovski, and E.R. Dufresne. 2013. Surfactant treatments influence drying mechanics in human stratum corneum. J. Biomech. 46: 2145–2151.

35. Ní Annaidh, A., K. Bruyère, M. Destrade, M.D. Gilchrist, and M. Otténio. 2012. Characterization of the anisotropic mechanical properties of excised human skin. J. Mech. Behav. Biomed. Mater. 5: 139–148.

36. Langer, K. 1861. On the anatomy and physiology of the skin: The cleavability of the cutis. Br. J. Plast. Surg. 31: 3–8.

37. Takahashi, M., K. Kawasaki, M. Tanaka, S. Ohta, and Y. Tsuda. 1981. The mechanism of stratum corneum plasticization with water. In: Bioengineering and the Skin. Springer. pp. 67–73.

38. Koutroupi, K.S., and J.C. Barbenel. 1990. Mechanical and failure behaviour of the stratum corneum. J. Biomech. 23: 281–287.

39. Gasperini, A.E., S. Sanchez, A.L. Doiron, M. Lyles, and G.K. German. 2017. Non-ionising UV light increases the optical density of hygroscopic self assembled DNA crystal films. Sci. Rep. 7.

40. Oyama, Z., Y. Naoe, H. Kimura, T. Masunaga, M. Seishima, Y. Aoyama, and Y. Kitajima. 2010. New non-invasive method for evaluation of the stratum corneum structure in diseases with

1   abnormal keratinization by immunofluorescence microscopy of desmoglein 1 distribution in tape-

2   stripped samples. J. Dermatol. .

3   41.   Naoe, Y., T. Hata, K. Tanigawa, H. Kimura, and T. Masunaga. 2010. Bidimensional analysis of

4   desmoglein 1 distribution on the outermost corneocytes provides the structural and functional

5   information of the stratum corneum. J. Dermatol. Sci. .

6   42.   Yokouchi, M., T. Atsugi, M. Van Logtestijn, R.J. Tanaka, M. Kajimura, M. Suematsu, M. Furuse,

7   M. Amagai, and A. Kubo. 2016. Epidermal cell turnover across tight junctions based on Kelvin's

8   tetrakaidecahedron cell shape. Elife. 5: e19593.

9   43.   ASTM G173-03(2012). 2012. Standard Tables for Reference Solar Spectral Irradiances: Direct

10   Normal and Hemispherical on 37* Tilted Surface. Am. Soc. Test. Mater. : 1–21.

11   44.   Yashar, S.S., R. Gielczyk, L. Scherschun, and H.W. Lim. 2003. Narrow-band ultraviolet B

12   treatment for vitiligo, pruritus, and inflammatory dermatoses. Photodermatol. Photoimmunol.

13   Photomed. 19: 164–168.

14   45.   Kleinpenning, M.M., T. Smits, J. Boezeman, P.C.M. Van De Kerkhof, A.W.M. Evers, and M.J.P.

15   Gerritsen. 2009. Narrowband ultraviolet B therapy in psoriasis: Randomized double-blind

16   comparison of high-dose and low-dose irradiation regimens. Br. J. Dermatol. 161: 1351–1356.

17   46.   Tjioe, M., M.J.P. Gerritsen, L. Juhlin, and P.C.M. Van De Kerkhof. 2002. Treatment of vitiligo

18   vulgaris with narrow band UVB (311 nm) for one year and the effect of addition of folic acid and

19   vitamin B12. Acta Derm. Venereol. 82: 369–372.

20   47.   Kreuter, A., J. Hyun, M. Stücker, A. Sommer, P. Altmeyer, and T. Gambichler. 2006. A

21   randomized controlled study of low-dose UVA1, medium-dose UVA1, and narrowband UVB

22   phototherapy in the treatment of localized scleroderma. J. Am. Acad. Dermatol. 54: 440–447.

23   48.   De Rie, M.A., D.N.H. Enomoto, H.J.C. De Vries, and J.D. Bos. 2003. Evaluation of medium-dose

1   UVA1 phototherapy in localized scleroderma with the cutometer and fast Fourier transform

2   method. Dermatology. 207: 298–301.

3   49.   Kroft, E.B.M., N.J.G. Berkhof, P.C.M. van de Kerkhof, R.M.J.P. Gerritsen, and E.M.G.J. de Jong.

4   2008. Ultraviolet A phototherapy for sclerotic skin diseases: A systematic review. J. Am. Acad.

5   Dermatol. 59: 1017–1030.

6   50.   Diffey, B.L. 1983. A mathematical model for ultraviolet optics in skin. Phys. Med. Biol. 28: 647.

7   51.   Bruls, W.A.G., H. Slaper, J.C. van Der Leun, and L. Berrens. 1984. Transmission of human

8   epidermis and stratum corneum as a function of thickness in the ultraviolet and visible

9   wavelengths. Photochem. Photobiol. 40: 485–494.

10   52.   Wu, K.S., W.W. van Osdol, and R.H. Dauskardt. 2006. Mechanical properties of human stratum

11   corneum: effects of temperature, hydration, and chemical treatment. Biomaterials. 27: 785–795.

12   53.   Wildnauer, R.H., J.W. Bothwell, and A.B. Douglass. 1971. Stratum corneum biomechanical

13   properties I. Influence of relative humidity on normal and extracted human stratum corneum. J.

14   Invest. Dermatol. 56: 72–78.

15   54.   Papir, Y., K. Hsu, R.H. Wildnauer, K. Hsh, R.H. Wildnauer, K. Hsu, and R.H. Wildnauer. 1975.

16   The mechanical properties of stratum corneum: I. The effect of water and ambient temperature on

17   the tensile properties of newborn rat stratum corneum. Biochim. Biophys. Acta (BBA)- …. 399:

18   170–180.

19   55.   Liu, X., J. Cleary, and G.K. German. 2016. The global mechanical properties and multi-scale

20   failure mechanics of heterogeneous human stratum corneum. Acta Biomater. 43: 78–87.

21   56.   Alonso, a, N.C. Meirelles, V.E. Yushmanov, and M. Tabak. 1996. Water increases the fluidity of

22   intercellular membranes of stratum corneum: correlation with water permeability, elastic, and

23   electrical resistance properties. J. Invest. Dermatol. 106: 1058–1063.

57. Kitajima, Y. 2015. Implications of normal and disordered remodeling dynamics of corneodesmosomes in stratum corneum. Dermatologica Sin. .

58. Jonca, N., M. Guerrin, K. Hadjiolova, C. Caubet, H. Gallinaro, M. Simon, and G. Serre. 2002. Corneodesmosin, a component of epidermal corneocyte desmosomes, displays homophilic adhesive properties. J. Biol. Chem. .

59. Johnson, J.L., J.L. Koetsier, A. Sirico, A.T. Agidi, D. Antonini, C. Missero, and K.J. Green. 2014. The desmosomal protein desmoglein 1 aids recovery of epidermal differentiation after acute UV light exposure. J. Invest. Dermatol. .

60. Walkley, K. 1972. Bound water in stratium corneum measured by differential scanning calorimetry. J. Invest. Dermatol. .

61. Vyumvuhore, R., A. Tfayli, H. Duplan, A. Delalleau, M. Manfait, and A. Baiilet-Guffroy. 2013. Effects of atmospheric relative humidity on Stratum Corneum structure at the molecular level: Ex vivo Raman spectroscopy analysis. Analyst. .

62. Bruls, W.A.G., and J.C. Van Der Leun. 1984. Forward scattering properties of human epidermal layers. Photochem. Photobiol. .

63. Kolmel, K.F., B. Sennhenn, and K. Giese. 1990. Investigation of skin by ultraviolet remittance spectroscopy. Br. J. Dermatol. .

64. Hoffmann, K., K. Kaspar, P. Altmeyer, and T. Gambichler. 2000. UV transmission measurements of small skin specimens with special quartz cuvettes. Dermatology. .

65. Arundel, A. V., E.M. Sterling, J.H. Biggin, and T.D. Sterling. 1986. Indirect health effects of relative humidity in indoor environments. Environ. Health Perspect. .

66. Dai, A. 2006. Recent climatology, variability, and trends in global surface humidity. J. Clim. .

1 67.   Nin, M., N. Katoh, S. Kokura, O. Handa, T. Yoshikawa, and S. Kishimoto. 2009. Dichotomous

2   effect of ultraviolet B on the expression of corneodesmosomal enzymes in human epidermal

3   keratinocytes. J. Dermatol. Sci. .

4 68.   Watkinson, A., C. Harding, A. Moore, and P. Coan. 2001. Water modulation of stratum corneum

5   chymotryptic enzyme activity and desquamation. Arch. Dermatol. Res. .

6 69.   Redoules, D., R. Tarroux, M.F. Assalit, and J.J. Perié. 1999. Characterisation and assay of five

7   enzymatic activities in the stratum corneum using tape-strippings. Skin Pharmacol. Appl. Skin

8   Physiol. .

9 70.   Suzuki, Y., J. Koyama, O. Moro, I. Horti, K. Kikuchi, M. Tanida, and H. Tagami. 1996. The role

10   of two endogenous proteases of the stratum corneum in degradation of desmoglein-1 and their

11   reduced activity in the skin of ichthyotic patients. Br. J. Dermatol. 134: 460–464.

12